Journal of Power Sources 195 (2010) 7669–7676

Contents lists available at ScienceDirect

Journal of Power Sources

journal homepage: www.elsevier.com/locate/jpowsour

Electrochemical properties of nickel–aluminum layered double hydroxide/carbon composite fabricated by liquid phase deposition

Alexis Bienvenu Béléké, Minoru Mizuhata*

Department of Chemical Science and Engineering, Graduate School of Engineering, Kobe University, 1-1 Rokko, Nada, Kobe 657-8501, Japan

ARTICLE INFO

Article history:
Received 29 April 2010
Received in revised form 31 May 2010
Accepted 31 May 2010
Available online 8 June 2010

Keywords:
Layered double hydroxide
Nickel hydroxide
Batteries
Positive electrode
Active materials
Crystallinity

ABSTRACT

Nickel–aluminum layered double hydroxide/carbon (Ni–Al LDH/C) composites have been fabricated using a mixed solution of $\{Al(NO_3)_3{\cdot}9H_2O$ and $H_3BO_3\}$ as fluoride scavengers in the liquid phase deposition (LPD) process. The amount of divalent Ni^{2+} substituted by trivalent Al^{3+} within the lattice of α-$Ni(OH)_2$ was controlled by the concentration of $Al(NO_3)_3{\cdot}9H_2O$ solution. X-ray diffraction studies reveal pure phase Ni–Al LDH, isostructural and isomorphic to α-$Ni(OH)_2$ with higher interlayer distance. The electrochemical properties of the cathode materials containing 0, 8.6, 13.8, 17.8, 21.3 and 23.4 Al% were evaluated by the means of charge–discharge and cyclic voltammetry measurements. The overall comparison indicates that Ni–Al LDH/C composites have higher electrochemical performance than pure α-$Ni(OH)_2$/C composite. The cathode with 17.8 Al% exhibits the best performance at 1 C compared to other Al^{3+} contents; a much lower voltage plateau, well separated from the oxygen evolution at the end of the charging as well as a single flat and high discharge plateau with a discharge capacity of 376.9 mAh $g_{comp}{}^{-1}$. Short term durability test for 80 cycles showed that the electrode containing 13.8 Al% has the highest discharge rate at 2 C. The range of Al substitution 13.8–17.8 Al% provides a good electrochemical response.

1. Introduction

Layered double hydroxide (LDH) materials are ideally described by hydrotalcite, a natural anionic clay of the composition $Mg_6Al_2(OH)_{16}CO_3{\cdot}4H_2O$ with general formula $[M^{II}{}_{1-x}M^{III}{}_x(OH)_2]{\cdot}[A^{n-}{}_{x/n}{\cdot}yH_2O]$, $A^{n-} = OH^-$, $CO_3{}^{2-}$, $NO_3{}^-$, etc., in which the substitution of a certain fraction x of the divalent cations by trivalent cations gives rise to a net positive charge. The excess of charge is counterbalanced with anions present in the interslabs [1,2]. Due to their anion exchange property and capacity to intercalate anions, LDH materials have potential applications in catalysts [3], anion exchangers [4,5], precursors to oxides [6], magnetics [7,8], and electrodes for alkaline secondary batteries [9,10]. It has been demonstrated that α-nickel hydroxide (α-$Ni(OH)_2$), which is one of the two polymorphs of nickel hydroxide, structurally and functionally behaves as an anionic clay, and exchanges the intercalated anions for hydroxyl ions from the alkaline electrolyte [9]. From this point of view, the use of α-$Ni(OH)_2$ as active materials of the positive electrode is expected to generate superior electrochemical performance compared to β-$Ni(OH)_2$ [10] which is currently used in commercial nickel secondary batteries. However, α-$Ni(OH)_2$ is labile and it rapidly converts to β-$Ni(OH)_2$ during synthesis or in the presence of strong alkaline media [11]. The unique approach to stabilize α-$Ni(OH)_2$ is by partial substitution of some fractions of Ni^{2+} ions with trivalent metal additives such as Al [12,13], Co [14,15], Fe [16,17], Mn [18,19], Zn [20,21] and Cr [22] in the lattice of $Ni(OH)_2$. Among these metal, Al is considered as the best additive due to its good stability [13,23,24].

A wide variety of methods of preparation of LDHs including coprecipitation, ion exchange, rehydration using structural memory effect, hydrothermal, secondary intercalation, intercalation involving dissolution and re-coprecipitation procedures is known in the literature [25]. However, the method of choice depends on the purpose for which the LDH is to be used. For battery applications, although some common methods of fabrication of LDHs such as coprecipitation [26], hydrothermal [27] or electrochemical reactions [13] have been employed, none of these techniques has satisfactorily reached a viable step for practical applications in battery technology. Therefore, the ease of scaling up any new synthetic procedure is still appealing for industrial prospects. In this scope, we have developed a novel technique of synthesis of Ni–Al LDH for battery application, the so-called liquid phase deposition (LPD) method. The basic concepts of the LPD process have been described elsewhere [28–32] and the main reactions can be expressed as follows:

$$MF_x{}^{(x-2n)-} + nH_2O = MO_n + xF^- + 2nH^+ \quad (1)$$

* Corresponding author. Tel.: +81 78 803 6186; fax: +81 78 803 6186.
E-mail address: mizuhata@kobe-u.ac.jp (M. Mizuhata).

0378-7753/$ – see front matter © 2010 Elsevier B.V. All rights reserved.
doi:10.1016/j.jpowsour.2010.05.068

Table 1
Active materials specifications.

Sample no.	Al content in solution (molar ratio)	Al^{3+} content in sample (molar ratio)	LDH content in sample (wt%)	Active material weight (mg)
1	0	0	61.6	5.00
2	2.4%	8.6%	67.6	5.01
3	4.7%	13.8%	69.0	5.00
4	9.0%	17.8%	75.0	5.12
5	16.0%	21.3%	69.8	5.24
6	20.0%	23.4%	66.6	5.31

$$H_3BO_3 + 4HF = BF_4^- + H_3O^+ + 2H_2O \quad (2)$$

$$Al + 6HF = H_3AlF_6 + (3/2)H_2 \quad (3)$$

This technique offers the possibility to control the amount of Al and the composition. The conventional LPD procedure involves the combination of the hydrolysis of the ligand exchange reaction (Eq. (1)) with either H_3BO_3 (Eq. (2)) or Al (Eq. (3)) as F^- scavenger. In the past works, we have described the synthesis of α-$Ni(OH)_2$ thin films [33] and α-$Ni(OH)_2$/C composite [34] using boric acid as fluoride scavenger in the LPD process. In the prospect to make α-$Ni(OH)_2$/carbon composite a candidate for the active materials of the positive electrode of nickel secondary batteries, we have extended the work to its stabilization using a mixed solution on boric acid and $Al(NO_3)_3{\cdot}9H_2O$ to produce high purity and well crystallized Ni–Al LDH/C composite [35,36]. Carbon particles are used as substrate for deposition in the LPD process. However its choice as a conductive agent has been proven to be beneficial in the terms of enhancing the electronic conductivity of electrochemical devices, including batteries due to its highly accessible surface area, good electrical conductivity, chemical stability and mechanical strength [37–41]. The fabricated composites were characterized by high resolution transmission electron microscope (HRTEM), X-ray diffractions (XRD), diffuse reflectance Fourier Transform infrared spectroscopy (DRITFS), inductively coupled plasma-atomic emission spectroscopy (ICP-AES). The performance and short term cycle life of the cathode materials containing 0, 8.6, 13.8, 17.8, 21.3 and 23.4 Al% were evaluated by the means of charge–discharge measurements at 1 and 2 C rates, respectively. Cyclic voltammetry was applied at a scan rate of 1 mV s^{-1} to evaluate the reversibility of the electrodes.

2. Experimental

2.1. Materials

The Ni parent solution was prepared as follows: 120 g of $Ni(NO_3)_2{\cdot}6H_2O$ (Nacalai Tesque Inc.) was dissolved into 800 mL of ion exchange water (IEW) and, while keeping under stirring, ca. 50 mL of 33 vol% of aqueous NH_3 (Nacalai Tesque Inc.) was dropwise added until pH reached 7.5. The collected precipitate was washed with IEW and dried at ambient temperature. It was then dispersed and agitated into 750 mL of 0.66 mol L^{-1} NH_4F (Nacalai Tesque Inc.) for 48 h at ambient temperature. The dispersion was filtered and the filtrate was adjusted with 0.66 mol L^{-1} NH_4F to make 30 mmol L^{-1} Ni parent solution. The fluoride scavenger starting solutions consisted of 0.5 mol L^{-1} H_3BO_3 and 0.05 mol L^{-1} $Al(NO_3)_3{\cdot}9H_2O$ (Nacalai Tesque Inc.). The initial Al/Ni ratios in solution as well as the Al^{3+} content in the composite are summarized in Table 1.

Oxidized carbon black (specific surface area: 58 m^2 g^{-1}) was used as substrate for the deposition. The oxidative pretreatment was carried out according to the same procedure as described in Ref. [34]. In typical procedure, 2.0 g of carbon black was first loaded in a bottomed flask set under refrigerant. Then 15.986 g of $KMnO_4$ was dissolved into 200 mL IEW by hot stirring for a few minutes, and loaded into a 500 mL mesh cylinder. Next, 132 mL of 4 mol L^{-1} HNO_3 solution was added on the $KMnO_4$ solution. The amount of the mixture was adjusted with IEW to make 400 mL solution which was poured on carbon black contained in the bottomed flask. The system was mixed by stirring at 70 °C for 4 h under refrigerant, filtrated and washed with hot IEW three times. The filtrate was shaken again in 400 mL of 2 mol L^{-1} HCl for 17 h at ambient temperature, washed with hot IEW twice, and dried at 110 °C for 8 h.

2.2. Composites preparation and characterization

Ni–Al LDH/C composite was prepared as follows: 20 mg oxidized carbon was loaded in a plastic bottle. Therein 40 mL of Ni parent solution containing [Ni^{2+}] of 30 mmol L^{-1} and [NH_4F] of 0.66 mol L^{-1}, 20 mL of 0.5 mol L^{-1} H_3BO_3 and 0.6–12 mL of 0.05 mol L^{-1} $Al(NO_3)_3{\cdot}9H_2O$, respectively, adjusted with IEW in 100 mL volumetric mesh flask were poured on. The final concentrations of Ni^{2+} and H_3BO_3 in the reaction solution were 12 mmol L^{-1} and 0.1 mol L^{-1}, respectively, while those of $Al(NO_3)_3{\cdot}9H_2O$ varied from 0.3 to 3 mmol L^{-1}. The mixture was shaken ultrasonically until carbon particles are completely dispersed in the reaction solution, and dived into water bath to allow reaction at 50 °C for 48 h. The sample was collected by suction filtration, washed repeatedly with hot IEW and dried at 50 °C for 3 h. For comparison purpose, pure α-$Ni(OH)_2$/C composite was synthesized by the same procedure without addition of Al solution.

The concentrations of Ni and Al contained in the composite or parent solution were determined by inductively coupled plasma-atomic emission spectroscopy (ICP-AES, HORIBA Ltd., ULTIMA 2000). For the composite, 5 mg was ultrasonically dispersed into 50 mL of diluted HNO_3 solution (0.26 mol L^{-1}), and stored in the oven at 50 °C for 48 h to allow dissolution of Ni and Al. The dispersion was then filtrated to remove carbon, and the filtrate was used for the measurements as sample.

The nature of anionic species contained in the composites was investigated by diffuse reflectance Fourier Transform infrared spectroscopy (DRIFTS) using FT-IR 615 type Spectrophotometer (JASCO), coupled with a diffuse reflectance attachment DR-600B (JASCO). The crystalline structures of the composites were characterized using X-ray diffractometer (Rigaku RINT-TTR/S2). The surface morphologies were observed by field emission scanning electron microscope (JEOL JEM-6335F) and high resolution transmission electron microscopy (HRTEM, JEOL2010).

2.3. Electrochemical measurements

The positive electrode was fabricated as follows. 5 mg of composite was mixed with 20 mg of 2 g cm^{-3} polyvinyl alcohol (PVA) as binder to make a paste. The mixture was loaded into 1 cm × 1 cm nickel mesh, dried under vacuum at 80 °C for 1 h and, then pressed under a pressure of 20 MPa for 1 min using a programmed digital press (Sinto Digital Press, Japan). A 1.5 cm × 1.5 cm nickel mesh was used as counter electrode whereas Ag/AgCl into saturated KCl served as reference electrode. 6 mol L^{-1} KOH solution was employed as an electrolyte. Galvanostatic charge–discharge and cyclic voltammetry were operated on Voltalab (Radiometer Analytical S.A., PGZ402, France). Each cell was immersed into 6 mol L^{-1}

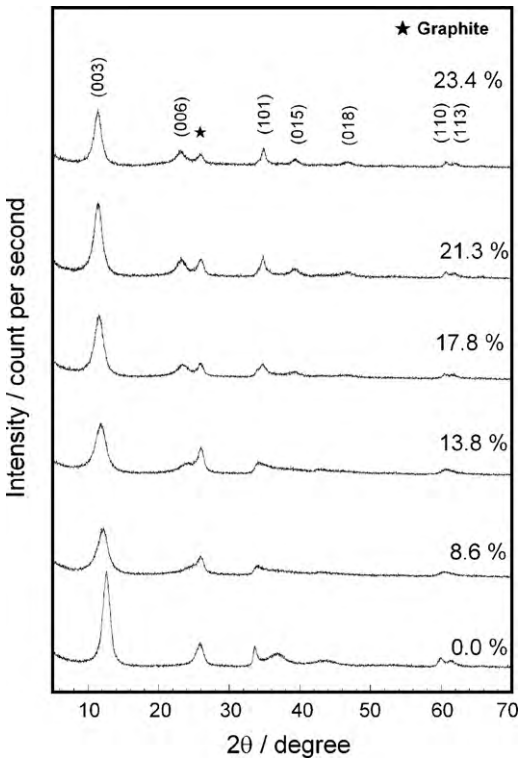

Fig. 1. XRD patterns of the as-prepared Ni–Al LDH/C composites at various Al contents.

KOH in an open circuit potential for 3 days prior to measurements to allow anion exchange procedure. It was then activated by charging and discharging at 5 C for 50 cycles. For the performance test, the cell was charged at 1 C for 1.2 h and discharge to 0 mV for 1 h. Cyclic voltammetry measurements were conducted at a scan rate of 1 mV s^{-1} versus Ag/AgCl after the performance test. All the electrochemical measurements were carried out at an ambient temperature.

3. Results and discussion

3.1. Analysis of the composite

The physical specifications of the as-prepared samples are summarized in Table 1. It can be noticed that the Al ratio contained in the composites is higher than the one in the reaction solution.

3.1.1. XRD studies

XRD patterns of the as-prepared Ni–Al LDH/C composites at various Al contents are shown in Fig. 1. All the Al-doped samples exhibit the same diffraction characteristics of Ni–Al LDH [10,13,42], isostructural to α-$Ni(OH)_2 \cdot 0.75H_2O$ (JCPDS card # 38-715). No peaks due to β-$Ni(OH)_2$ was detected. The peak intensities increase with increasing Al content. This aspect appears with more accuracy for the (0 0 6) reflection plane which coincides at the beginning (0 Al%) with the graphite peak around $2\theta = 25^\circ$, and then increased and shifted toward shorter 2θ values, indicating an increase in the interlayer distance. The variation of the (0 0 3) interlayer distance (d_{003}) and its peak relative intensity as a function of Al content is plotted in Fig. 2. (d_{003}) significantly increases with increasing Al^{3+} content up to 17.8% above of which further Ni substitution does not efficiently affect the structure of α-$Ni(OH)_2$ lattice. The (0 0 3) peak relative intensity can be used to assess the degree of crystallinity of the composite, the higher the intensity, the better the crystallinity [10]. The sample with 0 Al% exhibits the highest peak intensity.

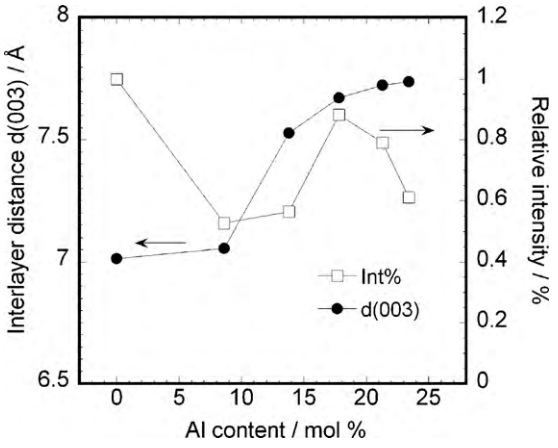

Fig. 2. Variation of (0 0 3) interlayer distance and relative intensity as a function of Al content.

The peak intensity of the LDH samples also increases with increasing Al^{3+} content up to 17.8%, then it decreases with higher Al^{3+} content. In sum, LDH samples displayed a poor crystallinity for the lower and higher Al^{3+} contents, while a better crystallinity could be achieved for the sample 17.8 Al%. This result suggests that the crystallinity of the composite does not depend on the Al^{3+} content in the LPD process.

Typical XRD patterns of the 17.8 Al% composite as-prepared and after 90 days of immersion in 6 mol L^{-1} KOH are depicted in Fig. 3. The sample after 90 days showed similar features as the as-prepared one. No peaks due to β-$Ni(OH)_2$ was observed. This indicates both an excellent stability and a high purity. The as-prepared samples display broad bands in XRD patterns, which confirms a poorly ordered structure. The asymmetric nature of the (1 0 1) plane is an evidence of the formation of turbostatic phase usually observed in α-$Ni(OH)_2$ [43]. The peak intensities of the as-prepared samples are higher than those of the immersed ones, indicating that LDH with good crystallinity could be achieved under current synthetic conditions. The interlayer distance calculated from the (0 0 3) reflection plane increased from 7.67 to 7.78 Å after KOH immersion. Furthermore, the KOH treated sample shows narrow, sharp and more symmetrical peaks. These information demonstrate that structural modifications have occurred during the KOH treatment, leading to a more ordered structure [10].

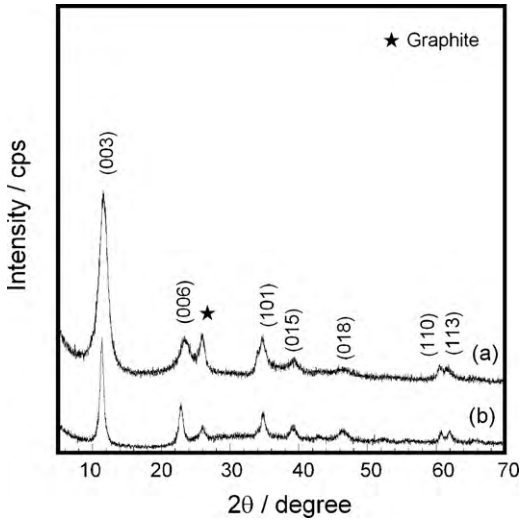

Fig. 3. XRD patterns of the 17.8 Al% composites: (a) as-prepared, (b) after 90 days of immersion in 6 mol L^{-1} KOH at ambient temperature.

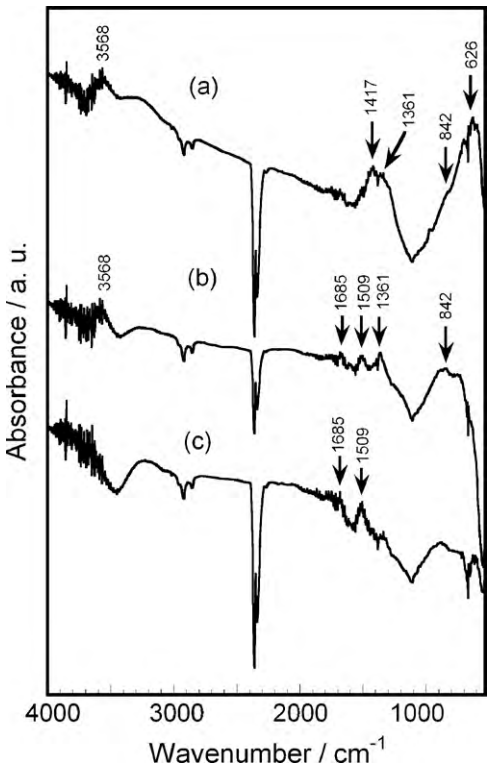

Fig. 4. Diffuse reflectance FT-IR spectra of the Ni–Al LDH/C composites: (a) 17.8 Al% as-prepared; (b) 17.8 Al% after 90 days of immersion in 6 mol L^{-1} KOH; (c) oxidized carbon

3.1.2. Infrared studies

Infrared spectra of the as-prepared and immersed samples are shown in Fig. 4. For comparison purpose, the spectrum of the oxidized carbon is also depicted. The spectrum of the as-prepared samples (Fig. 4a) displays the following features: (i) in the region of higher wavenumber (3600–3000 cm^{-1}), the band at 3568 cm^{-1} is attributed to the free hydroxyl groups while the broad band at 3430–3270 cm^{-1} represents the molecular vibration modes of hydrogen-bonded hydroxyl groups and water molecules; (ii) the broad vibrations in the 1550–1100 $cm^{-1}$are due to intercalated anions ions; and (iii) the 800–530 cm^{-1} region contains adsorbed species as well as M–O–OH bending vibrations [43–46]. The band with maximum peak at 1417 cm^{-1} is assigned to nitrates ions bound to Ni metal in C_{2v} symmetry while the one at 1361 cm^{-1} belongs to free nitrates ions (D_{3h} symmetry) in the interlayer gallery. The possible presence of anions such as tetrafluoroborates (BF_4^-) and/or tetrafluoroaluminates (AlF_4^-) adsorbed on the external surface of the crystallinities cannot be neglected because they are involved in the reaction mechanism of the deposition in the LPD process. Some of their characteristic frequencies, BF_4^- (A_1 777 cm^{-1}; T_2, 533 cm^{-1}) and AlF_4^- (A_1 622 cm^{-1}; T_2, 760 cm^{-1}) [47] may be overlapped or shadowed at 800–530 cm^{-1} while some other may take place at even lower wavenumber region beyond the measured range [48]. In the later case, it is very difficult to find precise assignment of these species because they are combined either to the lattice or to anions NO_3^- or OH^- [49]. With this consideration, the band at 626 cm^{-1} could be attributed to the A_1 mode of AlF_4^-. After 90 days, the free hydroxyl absorption at 3568 cm^{-1} remained unchanged while the broad band centered at 3400 cm^{-1} in the as-prepared spectrum vanished. The broad absorption in the 1550–1100 cm^{-1} also disappeared, leaving small bands at 1509 and 1361 cm^{-1}. The band at 1509 cm^{-1} belongs to unknown species derived from the oxidative pretreatment of carbon while the free nitrate band at 1361 cm^{-1} remained unperturbed. The intensity of the band at 1361 cm^{-1} considerably decreased, indicating a depletion of the amount of free nitrates ions. In the lower wavenumber region, the very strong absorption with maximum peak at 626 cm^{-1} disappeared, giving rise to a broad band with a maximum peak at 842 cm^{-1} assigned to ν_2 mode of the free NO_3^- [50]. It is assumed that this absorption contains bending mode of M–O–H along with unknown species belonging to the oxidized carbon surface. These results suggest that extra anions exist in the gallery space of the as-prepared samples, and such an excess has been exchanged with OH^- ions upon immersion in KOH, leading to a more ordered structure [10]. The presence of extra anions is expected to obstruct the proton diffusion during electrochemical processes.

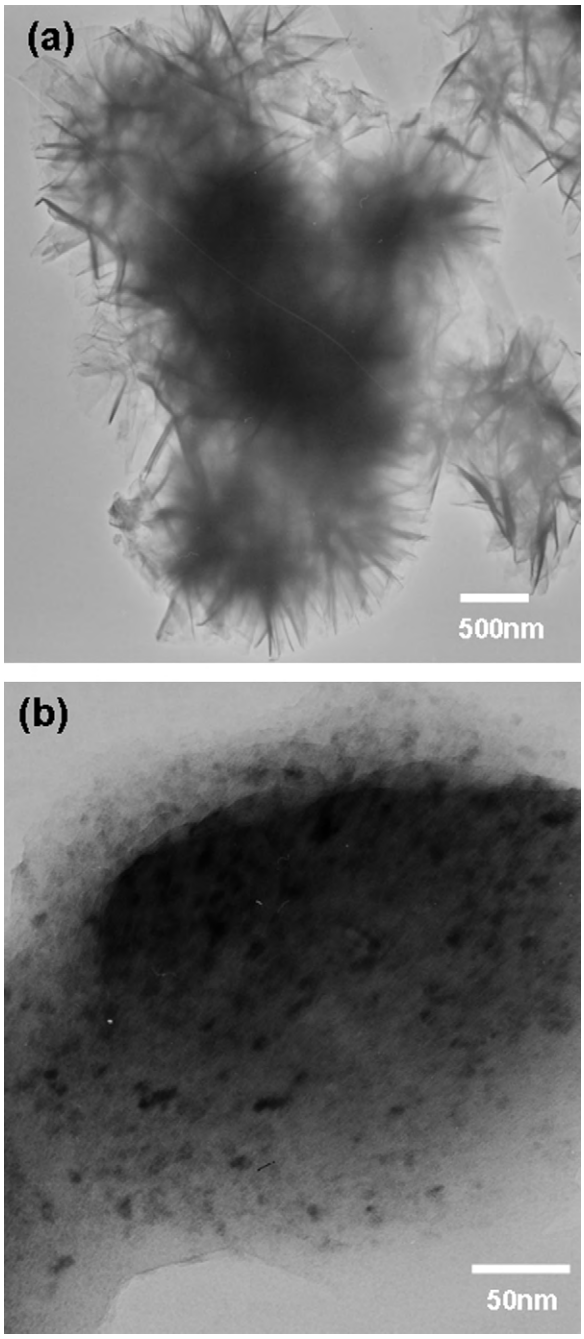

Fig. 5. High resolution TEM images of the as-prepared Ni–Al LDH/C composite containing 17.8 Al% at different magnitudes: (a) 500 nm; (b) 50 nm.

Fig. 5 illustrates the HRTEM image of the as-prepared Ni–Al LDH/C composite. Features in Fig. 5a appear as aggregates of thin

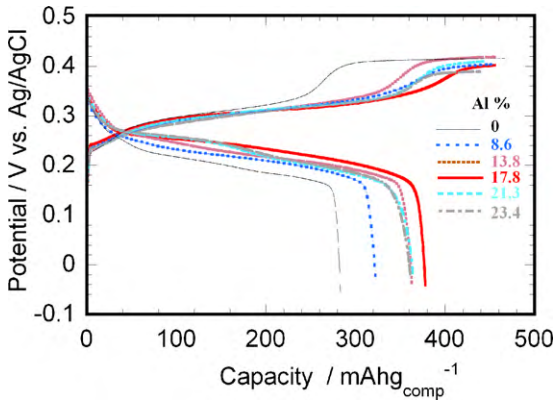

Fig. 6. Charge–discharge curves at 1 C rate of the electrodes with various Al contents.

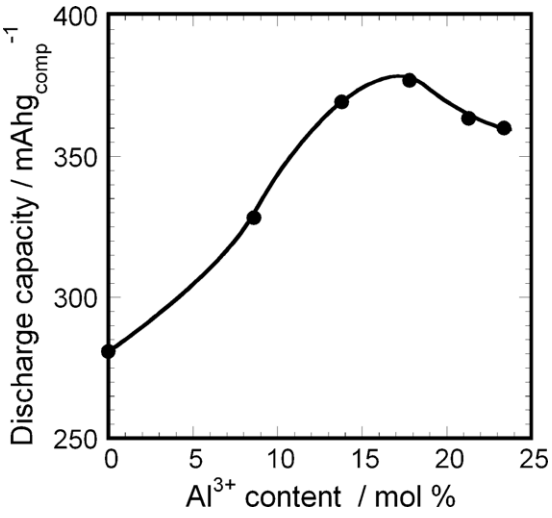

Fig. 7. Variation of the discharge capacities at 1 C as a function of Al content.

crumpled sheet without definite shape, usually observed for turbostatic materials [43,44]. The presence of carbon can be confirmed in Fig. 5b. The corresponding SEM image (see supporting information) indicates the same surface morphology as for samples prepared using different fluoride scavengers [34].

3.2. Electrochemical properties

It is noteworthy to mention that the capacity in this study is expressed in milliampere-hour per gram (mAh g_{comp}^{-1}) of composite rather than per gram of Ni because it is very difficult to determine with exactitude the amount of Ni contained in the composite due to loss during the processing.

3.2.1. Performance test

Fig. 6 shows the 15th charge–discharge curves at 1 C of the electrodes containing 0, 8.6, 13.8, 17.8, 21.3 and 23.4 Al%. The electrode containing 0 Al% presents a poor performance compared to all the LDH samples. This poor performance is probably caused by the structural transformation from α- to β-$Ni(OH)_2$ occurred during the conditionings and activation period. The discharge capacity of 280 mAh g_{comp}^{-1} which is so close to the theoretical capacity of β-$Ni(OH)_2$ (289 mAh g^{-1}) confirms this assumption. As it can be seen in Fig. 6, all the LDH samples exhibit similar trends on the charging: the electrode with 17.8 Al% shows a low and large voltage plateau, well separated from the oxygen evolution reaction at the end of the charging. On the discharging process, electrodes containing 8.6–17.8 Al% shows the same features: a single and flat discharge plateau lying between 270 and 190 mV vs Ag/AgCl. Among them, the electrode with 17.8 Al% presents the highest discharge voltage plateau whilst the one with the lowest Al content (8.6 Al%) gives the lowest discharge voltage plateau. However, the electrodes containing 21.3 and 23.4 Al% show two discharge plateaus, indicating the existence of two redox reactions.

The variation of the discharge capacity as a function of the Al content is plotted in Fig. 7. The discharge capacity increases with increasing Al content up to 17.8% and decreases. A discharge capacity of 376.9 mAh g_{comp}^{-1} could be achieved at 1 C for the electrode with 17.8 Al%, which corresponds to a number of exchanged electron of 1.3 per atom of Ni contained in a gram of composite. The increased number of exchanged electron can be attributed to the high phase purity and good stability of the active materials, since only the α/γ redox couples are involved in the charge–discharge process. In such a system it is known that on discharging from γ-NiOOH to α-$Ni(OH)_2$, it is possible to exchange up to 1.6 electrons. This is because the nickel atoms in γ-NiOOH have an average oxidation state of 3.6 due to some nickel atoms found in a +4 oxidation state [51]. Since the LDHs stabilize the α-nickel hydroxide phase, cycling between the α-$Ni(OH)_2$ and the γ-NiOOH can occur and more electrons can be exchanged [52]. The highest discharge capacity obtained in this work is very close to that of 20.4% Al-substituted α-$Ni(OH)_2$ hollow spheres [53]. The feature in Fig. 7 has similar tendency as the one observed in Fig. 2 for the relative intensity of the (0 0 3) reflection plane, suggesting a correlation between the performance and the crystallinity [10]. Therefore, the higher performance of the electrode containing 17.8 Al% could be attributed to the better crystallinity which basically depends on the carbon content. This aspect is under investigations and it will be discussed in a different work. Another hypothesis supporting the good performance of the electrode with 17.8 Al% could be a better balance between intercalated anions and water molecules within the interlayer space of α-$Ni(OH)_2$ lattice, which might be favorable to the proton diffusion during charge–discharge processes [24,26]. The optimal Al content of 17.8% found in this work is so close to those obtained within the range 18.3–20.4 Al% by different methods [26,53–56].

The origin of the second discharge voltage plateau has been investigated by several authors. Sac-Epée et al. [57] have demonstrated that the second voltage plateau is directly linked to the amount of γ-phase present in the nickel oxyhydroxide electrode (NOE) prior to its discharge. The authors also stated that the occasional appearance of this phase in the electrode results from a poor active material/current collector interface related to the electrode-forming technology, or to secondary reactions that can lead to a physical disconnection of the active material upon cycling. Electrochemical impedance spectroscopy study of the second plateau by Bardé et al. [58] has shown that the impedance becomes more capacitive at the second plateau, implying that proton diffusion is restricted. In our case; the appearance of two discharge voltage plateau for these electrodes with high Al^{3+} content is mainly attributed to slower proton diffusion in these materials compared to others. It is well known that the interlayer distance of α-$Ni(OH)_2$ is much more higher than that of β-$Ni(OH)_2$, which makes the diffusion of H^+ much easier. When the Al content increases, the intercalated anions (such as NO_3^- and CO_3^{2-}) obstruct the H^+ transport in the interslab, leading to a decrease of the diffusion coefficient of proton [56]. The combination of a low charge plateau on charging with the high discharge plateau on discharging, suggests the sample with 17.8 Al% has smaller polarization during charge and discharge [59].

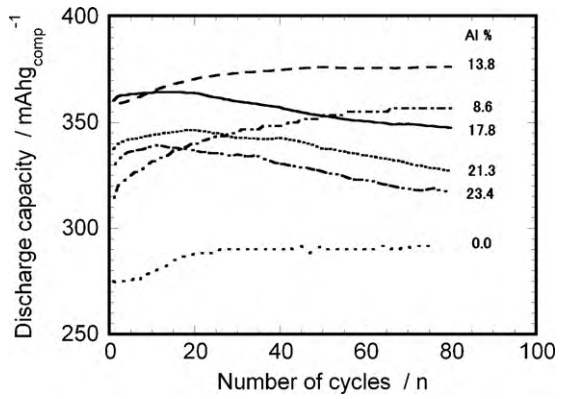

Fig. 8. Cycle performance of Ni–Al LDH/C electrodes with various Al contents.

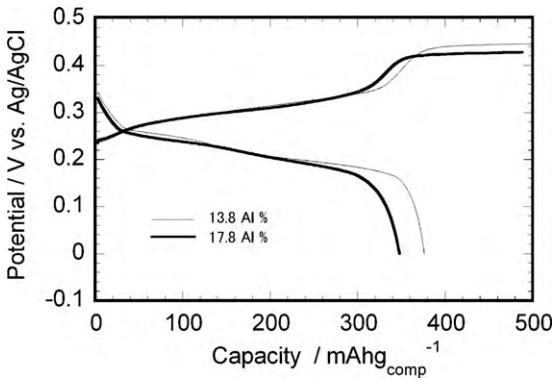

Fig. 10. Charge–discharge curves at 2 C rate of Ni–Al LDH/C electrodes containing 13.8 and 17.8 Al%.

3.2.2. Durability test

A short term cyclic performance of the electrodes has been investigated by charging and discharging at 2 C for 80 cycles. The evolution of the discharge capacity as a function of the cycle number is shown in Fig. 8. All the electrodes evolve in two steps. The first step consists of an increase of the discharge capacity up to the maximum, which corresponds to the activation time. The second step starts from the maximum value until the end of the cycle, which determines the discharge rate of the electrode. The variation of the discharge capacity at 2 C of the 80th cycle (75th for 0 Al% sample) as a function of the Al content is illustrated in Fig. 9. The discharge capacity of the electrode with 17.8 Al% at the beginning is the highest (360 mAh g_{comp}^{-1}). It rapidly increases and reaches its maximum at the 8th cycle, then starts fading from the 20th cycle. A similar cycle performance was obtained for 20 Al% by Morishita et al. [55]. The discharge capacity of the electrode with 13.8 Al% starts at 360 mAh g_{comp}^{-1}, reaches its maximum at the 50th cycle and ends up with a constant value of 376.7 mAh g_{comp}^{-1}. Such a high discharge capacity obtained at 2 C suggests that LPD-prepared Ni–Al LDH/C can be used as high rate discharge electrode materials [57]. The electrodes with 21.3 and 23.4 Al% also display a similar behavior without any constant step; their discharge capacities reach the maximum at the 18th and 10th cycles for 21.3 and 23.4 Al%, respectively, and start fading soon after. Finally, the sample with the lowest Al content shows the longest activation time (70th cycle). Accordingly, it appears that in the range from 13.8 to 17.8 Al% results in a good performance at both 1 and 2 C rates. This constitutes the optimal range of Ni^{2+} substitution by Al^{3+} in the LPD process. In the following study we focus on the range 13.8–17.8 Al%.

Fig. 10 shows the charge–discharge curves of the 80th cycle of the electrodes containing 13.8 and 17.8 Al% at 2 C. All the electrodes exhibit a similar tendency on the charging; a slightly slower and higher oxygen evolution reaction for the electrode with 13.8 Al% than that of 17.8 Al%. On the discharge, the electrode with 17.8 Al% maintains a better electrochemical response with a single flat discharge voltage plateau, which is in good agreement with the discharge behavior at 1 C rate. These information corroborate the optimal range of 13.8–17.8 Al% for the LPD-prepared active materials, which is somewhat higher than the results obtained by Hu and Noréus [24] for 10 Al% prepared by chemical precipitation. Although Zhao et al. obtained a high discharge capacity at 0.1 C for their sample containing 13.2 Al%, that sample was labile and easily converted to β-$Ni(OH)_2$ in 6 mol L^{-1} KOH at 45 °C [53]. In most of cases, electrodes made with active materials containing 10–15 Al% display poor performance because they are instable in strong alkali. Therefore, the interval 18.3–20.4 Al% appears to be the suitable range of Ni substitution when the materials are prepared with different methods [26,53–56]. This finding implies that the control of the Al^{3+} content depends on the preparation method.

3.2.3. Cyclic voltammetry

Cyclic voltammograms of the electrodes containing 13.8 and 17.8 Al% measured at a scanning rate of 1 mV s^{-1} after charge–discharge at 1 C are shown in Fig. 11. It can be seen that all the voltammetric curves present similar trends; a unique couple of anodic (oxidation) and cathodic (reduction) peaks is observed for each electrode. The anodic peaks slightly increase towards a more

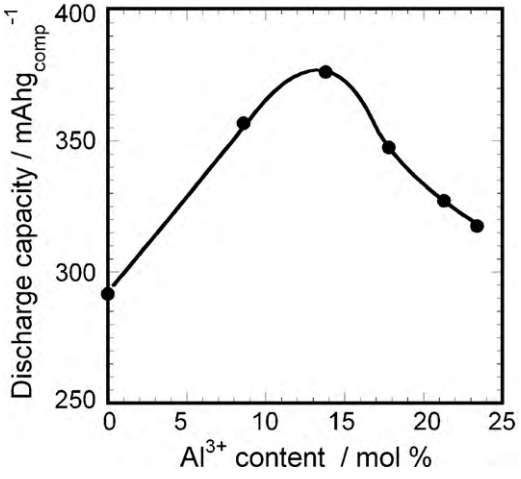

Fig. 9. Evolution of the discharge capacity at 2 C rate of the 80th cycle (75th cycle for 0 Al%) as a function of Al^{3+} content.

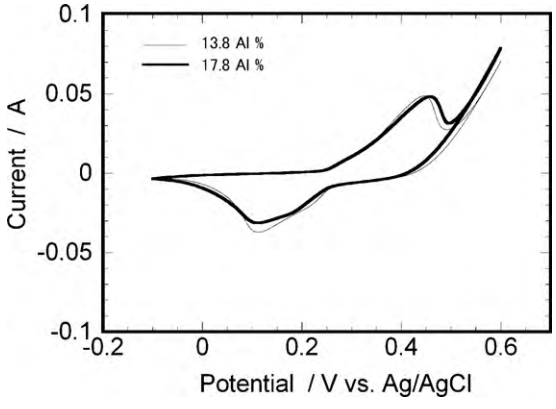

Fig. 11. Cyclic voltammograms of Ni–Al LDH/C electrodes containing 13.8 and 17.8 Al% measured at a scan rate of 1 mV s^{-1} after charge–discharge at 1 C rate.

Table 2
Cyclic voltammetry numerical data of the electrodes obtained after charge–discharge measurements at 1 C rate.

Samples	E_a (mV)	E_c (mV)	$\Delta E_{a,c}$ (mV)
13.8 Al%	446.3	111.8	334.5
17.8 Al%	358.3	111.8	346.5

E_a, anodic potential; E_c cathodic potential; $\Delta E_{a,c} = E_a - E_c$.

positive potential with increasing Al^{3+} content from 13.8 to 17.8 Al%, which is in good agreement with the charge–discharge behavior at 1 C. The CV numerical values are summarized in Table 2. $\Delta E_{a,c}$, defined as the potential difference between the anodic and cathodic peaks, is used as a measure of the reversibility of the electrochemical redox reaction: the higher the reversibility, the smaller $\Delta E_{a,c}$ is [60]. However, in all the cases, $\Delta E_{a,c}$ is higher than the theoretical value of 158 mV, which means that none of these electrodes is reversible [61]. These voltammograms have similar trends as those reported by Hu and Lei [62].

The overall performance of the LPD-prepared Ni–Al LDH/C composite active materials presented in this work is very encouraging, considering that this is the first time to apply such a new synthetic route to LDH materials. It is well known that the electrochemistry of layered double hydroxides depends on various parameters such as the effects of intercalated species, the degree of crystallinity, crystal morphology, defects and additives which have influence on the electrochemical properties [63]. Furthermore, the network-doping metal cations can enhance the electronic conductivity of the material, whereas introduction of interlayer anions can modulate its anionic conductivity [64]. All of these parameters are yet to be understood. A better handling of the electrochemical properties requires the improvement of the preparation technique in order to reduce some complexities. This is the goal behind this work whose primary objective is to make Ni–Al LDH/C composite effective active materials for Ni-MH batteries.

4. Conclusion

Ni–Al LDH/C composites have been successfully fabricated by the LPD method using a mixed solution of $\{Al(NO_3)_3{\cdot}9H_2O$ and $H_3BO_3\}$ as F^- scavenger. The as-prepared samples exhibited both good chemical and electrochemical stability. The cathode containing 17.8 Al% displayed the highest performance at 1 C with a discharge capacity of 376.9 mAh $g_{comp}{}^{-1}$ corresponding to a number of exchanged electron of 1.3. This high performance is mainly attributed to the good crystallinity. On the other hand, the electrode with 13.8 Al% showed a better cycle performance at 2 C, suggesting that LPD-prepared Ni–Al LDH/C can be used as high rate discharge electrode materials. The Al content 13.8–17.8 Al% constitutes the optimal range of Ni^{2+} substitution by Al^{3+} in the LPD process. With further investigations, Ni–Al LDH/C composite is projected as potential candidate for the positive electrode active materials of rechargeable nickel based batteries.

Acknowledgment

This study was carried out as the Energy and Environment Technologies Development Projects; "Development of an Electric Energy Storage System for Grid-connection with New Energy Resources" supported by Kawasaki Heavy Industries (KHI) Ltd. and New Energy and Industrial Technology Organization (NEDO). A part of this study was supported by Grant-in-Aid for Scientific Research (B) (No.22350094). We are thankful to Professor Shigehito Deki of Professor Emeritus of Kobe University, and Professor Hiroshi Inoue and Dr. Eiji Higuchi of Osaka Prefecture University for helpful discussions.

Appendix A. Supplementary data

Supplementary data associated with this article can be found, in the online version, at doi:10.1016/j.jpowsour.2010.05.068.

References

[1] V.R. Allman, Chimia 24 (1970) 99–108.
[2] M. Intissar, R. Segni, C. Payen, J.P. Besse, F. Leroux, J. Solid State Chem. 167 (2002) 508–517.
[3] A.A. Bhattacharyya, G.M. Woltermann, J.S. Yoo, J.A. Karch, W.E. Cormier, Ind. Eng. Chem. Res. 27 (1988) 1360–1456.
[4] A. Nakahira, T. Kubo, H. Murase, IEEE Trans. Magnetics 43 (2007) 2442–2444.
[5] S.V. Prasanna, P.V. Kamath, C. Shivakumara, Mater. Res. Bull. 42 (2007) 1028–1039.
[6] D. Tichit, M.J.M. Ortiz, D. Francova, C. Gérardin, B. Coq, R. Durand, F. Prinetto, G. Ghiotti, Appl. Catal. A: Gen. 318 (2007) 170–177.
[7] M. Taibi, S. Ammar, N. Jouini, F. Fiévret, P. Molinié, M. Drillon, J. Mater. Chem. 12 (2002) 3238–3244.
[8] A. Nakahira, H. Murase, J. Appl. Phys. 101 (2007), 09N516-3.
[9] P.V. Kamath, G.H.A. Therese, J. Solid State Chem. 128 (1997) 38–41.
[10] A. Sugimoto, S. Ishida, K. Hanawa, J. Electrochem. Soc. 146 (1999) 1251–1255.
[11] A. Delahaye-Vidal, M. Figlarz, J. Appl. Electrochem. 17 (1987) 589–599.
[12] F. Portemer, A. Delahaye-Vidal, M. Figlarz, J. Electrochem. Soc. 139 (1992) 671–678.
[13] P.V. Kamath, M. Dixit, L. Indira, A.K. Shukla, V.G. Kumar, N. Munichandraiah, J. Electrochem. Soc. 141 (1994) 2956–2959.
[14] V.G. Kumar, N. Munichandraiah, P.V. Kamath, A.K. Shukla, J. Power Sources 56 (1995) 111–114.
[15] C. Delmas, J.J. Braconnier, Y. Borthomieu, P. Hagenmuller, Mater. Res. Bull. 22 (1987) 741–751.
[16] R.D. Armstrong, E.A. Charles, J. Power Sources 25 (1989) 89–97.
[17] L. Demourgues-Guerlou, J.J. Braconnier, C. Delmas, J Solid State Chem. 104 (1993) 359–367.
[18] L. Demourgues-Guerlou, C. Delmas, J. Power Sources 45 (1993) 281–289.
[19] L. Demourgues-Guerlou, C. Delmas, J. Electrochem. Soc. 143 (1996) 561–566.
[20] L. Indira, M. Dixit, P.V. Kamath, J. Power Sources 52 (1994) 93–97.
[21] C. Tessier, L. Guerlou-Demourgues, C. Faure, M. Basterreix, G. Nabias, C. Delmas, Solid State Ionics 133 (2000) 11–23.
[22] R.S. Jayashree, P.V. Kamath, J. Power Sources 107 (2002) 120–124.
[23] H. Chen, J.M. Wang, Y.L. Zhao, J.Q. Zhang, J. Solid State Electrochem. 9 (2005) 421–428.
[24] W.K. Hu, D. Noréus, Chem. Mater. 15 (2003) 974–978.
[25] J. He, M. Wei, B. Li, Y. Kang, D.G. Evans, X. Duan, in: D.M.P. Mingos (Ed.), Structure and Bonding, vol. 119, Layered Double Hydroxides, Springer, Berlin/Heidelberg, 2005, pp. 89–120.
[26] L.J. Yang, X.P. Gao, Q.D. Wu, H.Y. Zhu, G.L. Pan, J. Phys. Chem. C 111 (2007) 4614–4619.
[27] F. Yang, B.Y. Xie, J.Z. Sun, J.K. Jin, M. Wang, Mater. Lett. 62 (2008) 1302–1304.
[28] H. Nagayama, H. Honda, H. Kawahara, J. Electrochem. Soc. 135 (1988) 2012–2016.
[29] A. Hishinuma, T. Goda, M. Kitaoka, S. Hayashi, H. Kawahara, Appl. Surf. Sci. 48/49 (1991) 405–408.
[30] S. Deki, Hnin Yu Yu Ko, T. Fujita, K. Akamatsu, M. Mizuhata, A. Kajinami, Eur. Phys. J. D 16 (2001) 325–328.
[31] S. Deki, S. Iizuka, A. Horie, M. Mizuhata, A. Kajinami, Chem. Mater. 16 (2004) 1747–1750.
[32] S. Deki, S. Iizuka, K. Akamatsu, M. Mizuhata, A. Kajinami, J. Am. Ceram. Soc. 88 (2005) 731–736.
[33] S. Deki, A. Hosokawa, A.B. Béléké, M. Mizuhata, Thin Films Solids 517 (2009) 1546–1554.
[34] A.B. Béléké, A. Hosokawa, M. Mizuhata, S. Deki, J. Ceram. Soc. Jpn. 117 (2009) 392–394.
[35] M. Mizuhata, A. Hosokawa, A.B. Béléké, S. Deki, Chem. Lett. 38 (2009) 972–973.
[36] M. Mizuhata, A. Hosokawa, A.B. Béléké, S. Deki, ECS Trans. 19 (2009) 41–46.
[37] C. Delacourt, C. Wurm, L. Laffont, J.B. Leriche, C. Masquelier, Solid State Ionics 177 (2006) 333–341.
[38] D. Aurbach, M.D. Levi, G. Salitra, N. Levy, E. Pollak, J. Muthu, J. Electrochem. Soc. 155 (2008) A745–A753.
[39] C.H. Doh, C.W. Park, H.M. Shin, D.H. Kim, Y.D. Chung, S.I. Moon, B.S. Jin, H.S. Kim, A. Veluchamy, J. Power Sources 179 (2008) 367–370.
[40] M. Masas-Cabanas, J.C. Hernandez, V. Gil, M.L. Soria, M.R. Palacín, Ind. Eng. Chem. Res. 23 (2004) 4957–4963.
[41] W.K. Zhang, X.H. Xia, H. Huang, Y.P. Gan, J.B. Wu, J.P. Tu, J. Power Sources 184 (2008) 646–651.
[42] L. Lei, M. Hu, X. Gao, Y. Sun, Electrochim. Acta 54 (2008) 671–676.
[43] P. Olivia, J. Leonardi, D. Delmas, J.J. Braconnier, M. Figlarz, F. Fievret, A. de Guibert, J. Power Sources 8 (1982) 229–255.
[44] Y. Li, X. Xie, J. Liu, M. Cai, J. Rogers, W. Shen, Chem. Eng. J. 136 (2008) 398–408.
[45] M. Dixit, P.V. Kamath, J. Gopalakrishnan, J. Electrochem. Soc. 146 (1999) 79–82.
[46] A. Delahaye-Vidal, B. Beaudoin, N. Sac-Epée, K. Tekaia-Elhsissen, A. Audemer, M. Figlarz, Solid State Ionics 84 (1996) 239–248.

[47] K. Nakamoto, Infrared and Raman Spectra of Inorganic and Coordination Compounds 5th ed. Part A. Theory and Applications in Inorganic Chemistry, Wiley, New York, 1997.
[48] Z.P. Xu, H.C. Zeng, J. Phys. Chem. B 105 (2001) 1743–1749.
[49] K. Tekaia-Elhsissen, A. Delahaye-Vidal, P. Genin, M. Figlarz, P. Willmann, J. Mater. Chem. 3 (1993) 883–888.
[50] M.J. Hernandez-Moreno, M.A. Ulibarri, J.L. Rendon, C.J. Serna, Phys. Chem. Miner. 12 (1985) 34–38.
[51] W.E. Grady, K.I. Pandya, K.E. Swider, D.A. Corrigan, J. Electrochem. Soc. 143 (1996) 1613–1616.
[52] G.A. Caravaggio, C. Detellier, Z. Wronski, J. Mater. Chem. 11 (2001) 912–921.
[53] Y. Li, W. Li, S. Chou, J. Chen, J. Alloys Compd. 456 (2008) 339–343.
[54] Y.L. Zhao, J.M. Wang, H. Chen, T. Pan, J.Q. Zhang, C.N. Cao, Int. J. Hydrogen Energy 29 (2004) 889–896.
[55] M. Morishita, T. Kakeya, S. Ochiai, T. Ozaki, Y. Kawabe, M. Watada, T. Sakai, J. Power Sources 193 (2009) 871–877.
[56] H. Chen, J.M. Wang, T. Pan, Y.L. Zhao, J.Q. Zhang, C.N. Cao, J. Power Sources 143 (2005) 243–255.
[57] N. Sac-Epée, M.R. Palacin, B. Beaudoin, A. Delahaye-Vidal, T. Jamin, Y. Chabre, J.M. Tarascon, J. Electrochem. Soc. 144 (1997) 3896–3907.
[58] F. Bardé, P.L. Taberna, J.M. Tarascon, M.R. Palacin, J. Power Sources 179 (1998) 830.
[59] T. Pan, J.M. Wang, Y.L. Zhao, H. Chen, H.M. Xiao, J.Q. Zhang, Mater. Chem. Phys. 78 (2003) 711–718.
[60] W.H. Zhu, J.J. Ke, H.M. Yu, D.J. Zhang, J. Power Sources 56 (1995) 75–79.
[61] D.A. Corrigan, R.M. Bendert, J. Electrochem. Soc. 136 (1989) 723–728.
[62] M. Hu, L. Lei, J. Solid State Electrochem. 11 (2007) 847–852.
[63] J. Ren, Z. Zhou, X.O. Gao, J. Yan, Electrochim. Acta 52 (2006) 1120–1126.
[64] A. Doménech-Carbó, Electrochemistry of Porous Materials, CRC Press, Boca Raton, 2010, pp 117–142.